Article

Water Recuperation from Regolith at Martian, Lunar & Micro-Gravity during Parabolic Flight

Dario Farina [1,*], Hatim Machrafi [1,2], Patrick Queeckers [1], Christophe Minetti [1] and Carlo Saverio Iorio [1,*]

1 Centre for Research and Engineering in Space Technologies (CREST), Department of Aero-Thermo-Mechanics, Université Libre de Bruxelles, 1050 Bruxelles, Belgium
2 GIGA-In Silico Medicine, Université de Liège, 4000 Liège, Belgium
* Correspondence: dario.farina@ulb.be (D.F.); carlo.iorio@ulb.be (C.S.I.)

Abstract: Recent discoveries of potential ice particles and ice-cemented regolith on extraterrestrial bodies like the Moon and Mars have opened new opportunities for developing technologies to extract water, facilitating future space missions and activities on these extraterrestrial body surfaces. This study explores the potential for water extraction from regolith through an experiment designed to test water recuperation from regolith simulant under varying gravitational conditions. The resultant water vapor extracted from the regolith is re-condensed on a substrate surface and collected in liquid form. Three types of substrates, hydrophobic, hydrophilic, and grooved, are explored. The system's functionality was assessed during a parabolic flight campaign simulating three distinct gravity levels: microgravity, lunar gravity, and Martian gravity. Our findings reveal that the hydrophobic surface demonstrates the highest efficiency due to drop-wise condensation, and lower gravity levels result in increased water condensation on the substrates. The experiments aimed to understand the performance of specific substrates under lunar, Martian, and microgravity conditions, providing an approach for in-situ water recovery, which is crucial for establishing economically sustainable water supplies for future missions. To enhance clarity and readability, in this paper, "H_2O" will be referred to as "water".

Keywords: regolith hydration; water extraction technologies; parabolic flight simulation; ice-regolith interaction; substrate condensation efficiency; in-situ resource utilization (ISRU); thermal condensation processes; micro-gravity experiments; surface properties and water recovery; space resources; space mining

1. Introduction

Exploration of water on extraterrestrial bodies such as the Moon and Mars has heightened, encouraged by the confirmed presence of ice particles and ice-cemented regolith [1–3]. The study of water condensation under different gravity conditions is crucial because gravity influences various physical processes, such as fluid dynamics and phase transitions, which are essential for understanding and optimizing water recovery in extraterrestrial environments. Gravity affects the behavior of fluids by altering the convection currents and pressure distribution. In lower gravity, the lack of significant buoyancy forces leads to different fluid behaviors compared to Earth's gravity, impacting condensation and evaporation rates. Understanding these differences is key to designing efficient water recovery systems for space applications. These discoveries are not merely academic; they reshape our understanding of these bodies' geological past and create tangible stepping stones toward future space exploration and potential colonization [4,5]. In-Situ Resource Utilization (ISRU) or On-Site Resource Utilization is central to these efforts, enabling the extraction and use of local materials to support long-term human presence and activities on the Moon and Mars. ISRU techniques, such as extracting water from regolith and producing oxygen, play a vital role in making space missions more sustainable and cost-effective. By leveraging

local resources, we can significantly reduce the dependency on Earth supplies, paving the way for more ambitious and extended space missions, relevant studies include [6,7]. The presence of water ice was notably confirmed at the Moon's south pole by the Lunar Crater Observation and Sensing Satellite (LCROSS) mission and has been further evidenced by the observations of NASA's Lunar Reconnaissance Orbiter (LRO) [8,9]. Recent studies have highlighted the presence and potential for extraction of polar ice on the Moon, which could be a vital resource for future lunar missions [10]. On Mars, the Mars Reconnaissance Orbiter and the Phoenix Lander have provided compelling evidence of water-ice, particularly within shaded craters and sub-surface layers [11,12]. Recent studies have provided new insights and raised unresolved questions about Mars, highlighting the complexities and ongoing debates in astrobiological research on the planet [13]. Moreover, NASA's Stratospheric Observatory for Infrared Astronomy (SOFIA) detected molecular water on the sunlit surface of the Moon's Clavius Crater in October 2020, revealing that water molecules can withstand lunar surface conditions [14,15]. Building on this discovery, Liu et al. (2012) provided direct measurements of hydroxyl in the lunar regolith, offering further evidence of the persistence and stability of water molecules on the Moon's surface [16].

These findings contribute significantly to our understanding of the lunar hydrosphere and highlight the Moon's potential for sustaining water-based activities necessary for future human and robotic missions. Water is a critical resource for human survival, mission operations, and as a fuel component, making the establishment of reliable water extraction technologies a crucial challenge [17]. The unique conditions of the Moon, with water concentrations detected near the poles and in permanently shaded regions, particularly the lunar south polar region, have been identified as promising sites for water ice drilling missions [18], make it a promising candidate for In-situ Resource Utilization (ISRU) [19,20]. Similarly, Mars presents unique challenges and opportunities, with its regolith believed to contain bound H_2O molecules, which can be extracted to support long-duration human missions [21]. Additionally, the process of deliquescence, which allows the formation of liquid on Mars today, is significant in this context [22].

Numerous techniques have been proposed to extract water from extraterrestrial bodies, employing a variety of thermal and physical processes tailored to the specific conditions and forms of water present [23–25]. In scenarios where water exists as ice mixed with regolith, thermal sublimation is commonly applied. This method involves directly heating the ice-regolith mixtures to transform the ice into vapors, which are then captured [26,27]. The effectiveness of this technique has been demonstrated in controlled lunar simulations, illustrating how thermal energy can efficiently convert ice to vapor for collection.

Another promising technique is microwave heating, which has shown significant potential in laboratory settings. Unlike conventional heating methods, microwaves penetrate the regolith and directly excite water molecules, rapidly heating and sublimating the ice even when it is deeply embedded within the soil. This method is particularly advantageous for its efficiency, targeting water molecules specifically to minimize heat loss, and could be effectively adapted for lunar missions [28].

Hydrothermal processing represents a third approach, utilizing hot water or steam to heat the regolith and release water molecules. This method adapts terrestrial geothermal recovery techniques for extraterrestrial environments, offering a versatile solution tailored to different regolith compositions and water content levels [29]. By adjusting the temperature and pressure of the steam, hydrothermal processing can extract water from various forms of bound water in Martian permafrost or mineral hydrates.

Each of these techniques not only demonstrates the practicality of extracting H_2O in space environments but also highlights the adaptability of Earth-based technologies for use on extraterrestrial bodies [30]. The continued development and refinement of these methods are essential for advancing In-Situ Resource Utilization (ISRU) strategies, crucial for establishing sustainable human outposts on the Moon and Mars by leveraging local resources for life support, agriculture, and fuel production [31].

The method proposed in this study involves filling an empty evaporator (a device where regolith is placed and used to convert liquid into vapor with dimensions of $118 \times 58 \times 10$ mm) with a desired amount of icy-regolith, sealing the evaporator, and heating it. As the temperature of the regolith rises during this heating phase, water vapor is released, which then accumulates on a cooled substrate, facilitating the collection of extracted water. Using droplets for condensation is beneficial compared to bulk water or surface dew film as it allows for more precise control and measurement of the condensation process, leading to better efficiency and understanding of the underlying mechanisms. The methodology involves a detailed analysis of three distinct substrate types: hydrophobic, hydrophilic, and grooved surfaces (grooves are excavated at 5 mm depth and 5 mm width along a length of 58 mm), under simulated lunar, Martian, and micro-gravity conditions. These substrates were chosen based on their unique properties, which influence the behavior of H_2O molecules during the condensation process. The selection was informed by a comprehensive literature review, identifying these surfaces as promising candidates for enhancing water recovery rates [32–34]. However, despite various proposed techniques, there is a lack of available studies on water extraction and recuperation under reduced gravity conditions.

This study aims to evaluate the performance of specific substrates under different gravitational conditions: namely lunar, Martian, and microgravity environments. Each substrate type: hydrophobic, hydrophilic, and grooved—was tested at these three gravity levels to determine its effectiveness in water recovery from regolith simulants. The goal is to understand how gravity influences the condensation and recovery of water, providing insights essential for the development of efficient in-situ water recovery systems. By comparing the functionality of each substrate across the different gravitational environments, we aim to identify which substrate performs best under each condition. These insights are crucial for optimizing water extraction technologies and making future space missions more economically sustainable.

In this study, "parabolas" refer to the flight maneuvers performed by the aircraft to simulate different gravity levels. Each parabola consists of a series of phases, including a hypergravity phase, a reduced gravity phase, and a return to normal gravity, which allows for the study of water condensation under varying gravity conditions.

2. Materials and Methods

2.1. Experimental Setup and Procedure

The experimental setup is shown in Figure 1 while Figure 2 offers a 3D view. The casing is constructed primarily from Polyetheretherketone (PEEK), with the exception of the top and frontal viewing panels, which are fabricated from Plexiglass to facilitate observation. This enclosure is hermetically sealed to prevent external contamination and to allow for precise control of internal pressure, crucial for experimental integrity. A heater is attached to the lower surface of the evaporator to ensure even heat distribution. Temperature and pressure sensors are strategically placed within the enclosure to monitor experimental conditions continuously.

A JAI GO-5000M (DK-2500 Valby, Copenhagen, Denmark) camera is positioned externally, aligned with the condenser to document the condensation process. The enclosure dimensions ($210 \times 170 \times 160$ mm) were optimized for flight constraints and ensure effective shielding from external variables. Within this setup, 120 gr of highland regolith (OPRH3N, developed by Off Planet Research in Everett, WA, USA) was used, containing 80% anorthosite and 20% basaltic cinder mixed with 45 mL H_2O evenly spread inside the evaporator surface. The grain sizes of the regolith used and mixed are shown in Table 1. Prior to the experiment, the regolith simulant was thoroughly dried to remove any absorbed moisture, ensuring that the initial water content in the system was accurately controlled and solely from the added 45 mL of H_2O. Initially, the environmental pressure inside the sealed case is set at 4 millibars, a value chosen to balance the need for low pressure against the practical constraints of parabolic flight preparations, where lower pressures

would necessitate impractically extended preparation durations. Although this pressure is more applicable to Mars, our system operates in a closed environment isolated from external conditions. This isolation allows precise control over internal pressure, similar to a controlled lunar environment, facilitating the study of condensation processes. Controlling pressure in a closed system is advantageous for managing condensation, ensuring the relevance of our results to lunar conditions.
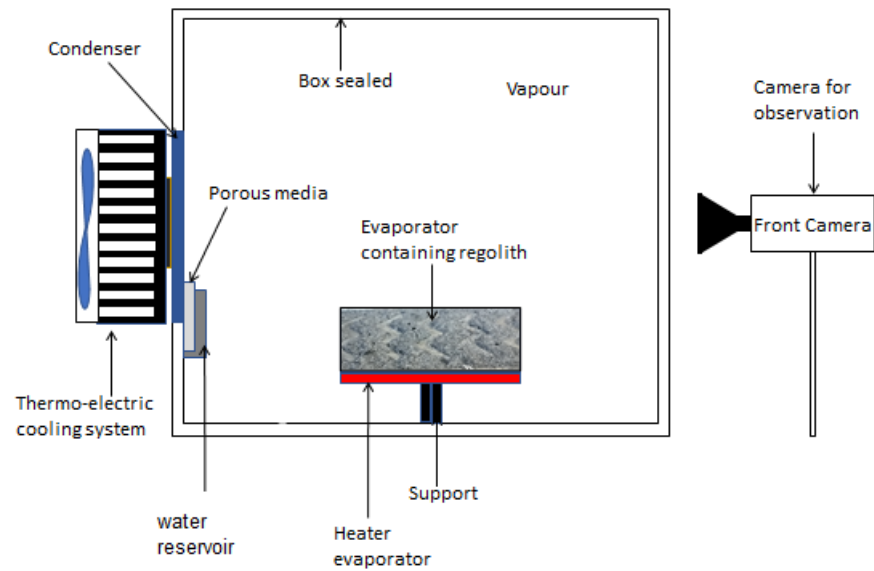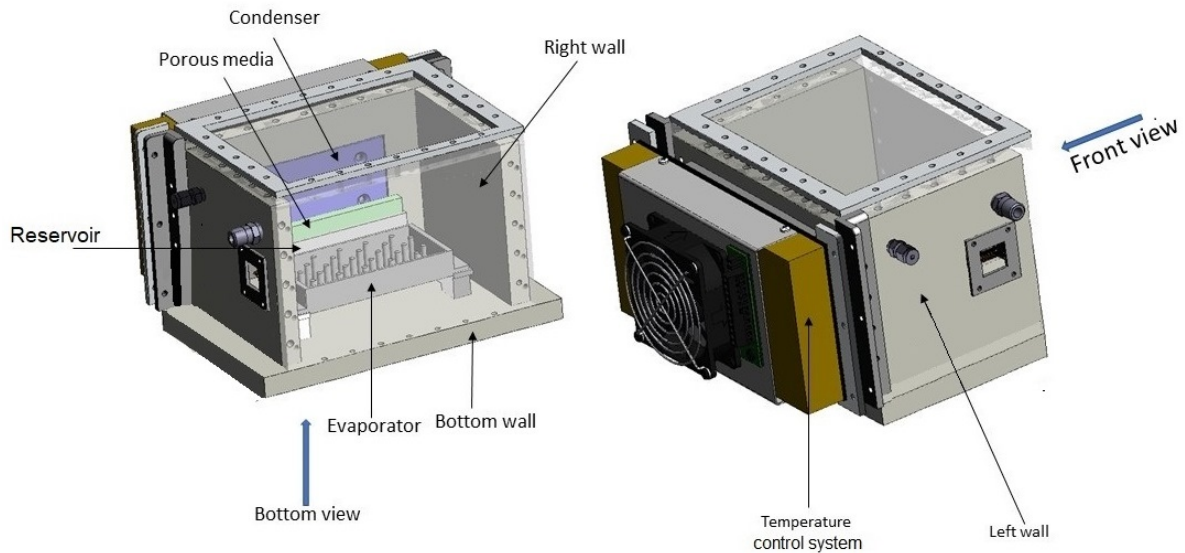

Figure 1. Scheme of the Experiment.

Figure 2. View of the setup used for the parabolic flight campaign.

Table 1. Grain sizes of the used regolith simulant.

Layer	Grain Size
Layer 1	Grain size 0.125 mm to 0.105 mm
Layer 2	Grain size 0.250 mm to 0.177 mm
Layer 3	Grain size 2 mm to 0.500 mm

The flight campaign involved a series of 30 parabolas each day, simulating microgravity, lunar gravity, and Martian gravity conditions. The aircraft maneuvered through a

controlled trajectory to achieve these conditions, carefully monitored by engine thrust. This dynamic flight pattern posed unique challenges for managing the condensed fluid. During hypergravity phases, fluid dispersal was chaotic, while in microgravity, condensate tended to float or form a thick film on the condenser plate, impeding condensation efficiency.

To address these challenges, porous media was strategically placed inside the reservoir below the condenser plate. This setup not only absorbed and channeled away fluid effectively but also prevented dispersion during hypergravity and inhibited thick film formation during microgravity phases. This ensured continuous and effective condensation across varying gravity conditions encountered during the parabolic flights.

The apparatus was equipped with a Peltier element, and a cooling system on the condenser plate to maintain desired temperature conditions, all controlled via a PID controller. Data from the sensors were logged using an Agilent 34970A data logger (Agilent Technologies, Santa Clara, CA, USA)..

The methodology involved rigorous preparation of regolith simulants, assembly of the experimental apparatus, and control during flight to investigate H_2O condensation dynamics effectively under varied gravitational conditions.

2.2. Ground Control Experiments

Before the parabolic flight experiments, ground control tests were conducted to establish baseline data and validate the experimental setup. These tests aimed to simulate similar conditions to those expected during parabolic flights but under stable terrestrial gravity. The objectives of the ground experiments were to evaluate the performance of the water recovery apparatus, assess the condensation efficiency on different substrates, and ensure the reliability of the temperature and pressure control systems.

In these tests, the environmental conditions, such as pressure and temperature, were meticulously controlled to replicate the experimental setup used during the parabolic flights. The regolith simulant was mixed with water and subjected to the same thermal and condensation processes. The results from these ground control experiments provided essential baseline data, allowing for a comparative analysis with the data obtained under varying gravity conditions during the parabolic flights. This approach ensured the consistency and accuracy of the experimental findings and facilitated the identification of any anomalies attributable to changes in gravity.

Additionally, several experiments were performed under ground conditions using the same procedures. These tests reproduced the entire duration of the flight, including the 2.5-h experimental period, to simulate the condensation process accurately. This approach demonstrated the influence of gravity and confirmed the stability of the condensation process, providing further validation of our experimental setup and findings.

2.3. Parabolic Flight Conditions

In December 2020, the 74th ESA parabolic flight campaign provided our team the opportunity to study H_2O recovery from lunar regolith in a simulated space environment. The experiments aimed to understand the performance of specific substrates under lunar, Martian, and microgravity conditions, key to future utilization of extraterrestrial resources.

The experimental apparatus was housed in a robust container (Zargas aluminium case), monitored to preserve experimental conditions throughout the flight. During the flight campaign, the aircraft was meticulously controlled to replicate Martian, lunar, and micro-gravity conditions for the experiments. It began with a normal 1 g phase, escalated to a 2 g hypergravity during a sharp ascent, and transitioned into various reduced gravity states mimicking lunar and Martian gravities, and microgravity during the parabolic arcs.

Each of the parabolas executed daily involved precise control over ascent to a 2 g state, maintenance of reduced gravity, and a return to 2 g before stabilizing at 1 g. The meticulous control over these phases ensured that each gravity level was sustained for specific durations necessary for the experiments. Figure 3 in the documentation illustrates these

transitions in gravity levels, altitude, and timing, showcasing the detailed management of experimental conditions.
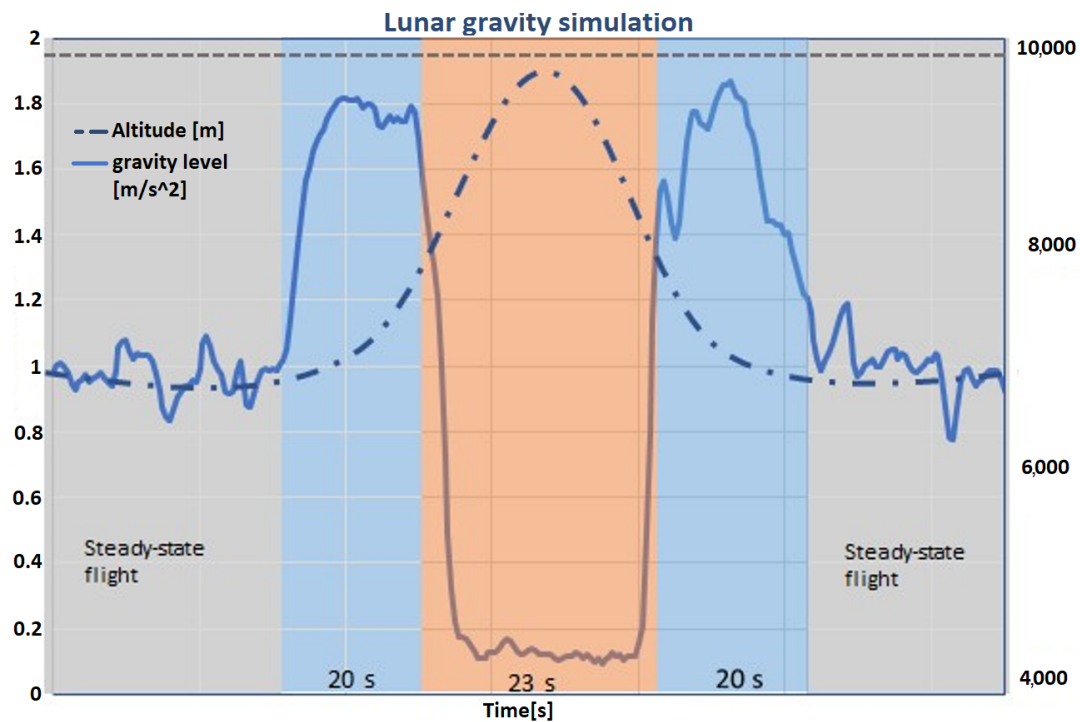

Figure 3. Gravity profile during the parabolic flight with respect to Earth Gravity.

Each day, the temperature in the condenser plate was held at a stable value of around 10 °C for the first fifteen parabolas and around 15 °C for the second group of fifteen parabolas. Some variation in the temperature was still observed due to unstable conditions of the parabolic flights and the constant variations in gravity (g-jitters), which made it challenging to keep a fixed value. Each day, one of the substrates was used (grooved, hydrophobic, or hydrophilic). For each day (equivalent to one substrate choice), Table 2 shows the composition of the flight corresponding to the reduced-gravity levels.

Table 2. Days flight composition.

Parabola	0–5	6–10	11–15	16–20	21–25	26–30
Grooves	0.38 g	0.16 g	0 g	0g	0.16 g	0.38 g
Hydrophobic	0 g	0.38 g	0.16 g	0.16 g	0.38g	0 g
Hydrophilic	0.16 g	0 g	0.38 g	0.38 g	0g	0.16 g

10°C   15°C

3. General Approach for the Image Analysis

3.1. Image Preparation

A Drop Shape Analyzed Kruss DSA30 is used for precise droplet contact angle measurements. The droplet contact angle is defined as the angle at which a liquid/vapor interface meets the solid surface. It quantitatively measures the wettability of a surface by a liquid. The results obtained helped in the analysis of the drop shape formed on the surface. Furthermore, as shown in Figure 4, the contact angle was measured to be 50° for the hydrophilic surface, 119° for the grooved substrate, and 116° for the hydrophobic one. These values are found in harmony with the definitions found in the literature of hydrophobic and hydrophilic surfaces [35]. It has been verified that by varying the contact

angle around the mentioned respective values for each respective type of substrate, during the image processing, the obtained condensation values appeared to vary negligibly, and The overall behavior observed in the analysis is therefore considered to remain consistent. Before resulting in the detection of condensed drops, the prepared images need to undergo individual tuning, depending on the type of substrate. The general process outlined in this section is illustrated in Figure 5. The same figure shows the application of a Fourier transform, which is used to analyze the spatial frequency of the condensation patterns on the condenser surface. This technique helps in understanding the distribution and periodicity of droplets formed during the experiment, providing insights into the efficiency and uniformity of the condensation process.

Figure 4. Contact angle (CA) measured on the top of the groove, as well as for the hydrophobic and hydrophilic.
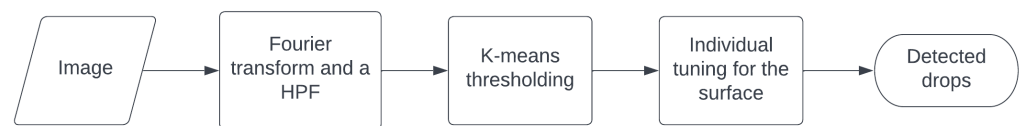

Figure 5. Generalization of the Droplet Volume Quantification Process.

Figure 6 shows the grooves substrate, chosen for the capability of the channels to have the double effect of increasing the surface for heat exchange and the implemented capabilities of removing the condense through their channels. A camera showed H_2O condensation for the substrates but no drop-wise condensation that was required for the analysis. The three substrates having uneven lighting, with drops not being uniform also caused trouble in this area. On the other hand, it can be seen that at least in the short-axis direction ('short-axis direction' refers to the direction along the shorter dimension of the evaporator or the observed surface), the individual droplets are by far the smallest feature in the picture, associated with much higher spatial frequencies than the lighting grooves or paths. To effectively filter out the lower spatial frequencies using a finely adjusted high-pass filter, the images were converted to the Fourier domain. Manual masking mitigated several challenges encountered in this approach, ensuring minimal impact on the final outcomes. This procedure was applied to the grooved substrate to illustrate the image analysis performed in this work. The same procedure was employed later on other substrates. Figure 6 illustrates the difference between the 'Original' image and the 'after HPF' (High-Pass Filter) image. The 'Original' image represents the raw visual data of the condensation on the condenser surface. The 'After HPF' image, on the other hand, has undergone a high-pass filter process to enhance the visibility of fine details by removing low-frequency components. This filtering technique emphasizes the edges and finer structures of the condensation patterns, allowing for a more detailed analysis of the droplet formation and distribution. Several thresholding algorithms were compared by applying k-means clustering to partition the data into two distinct groups, which yielded the most favorable outcomes. In this context, 'k' represents the number of clusters, determining the division of the data. Figure 7 shows the thresholded image of the grooved substrate, allowing us to evaluate the areas of individual droplets. These areas can be further transformed into droplet volumes, where it was assumed that all droplets have a paraboloid shape, where the droplet area corresponds to the area of the paraboloid base.
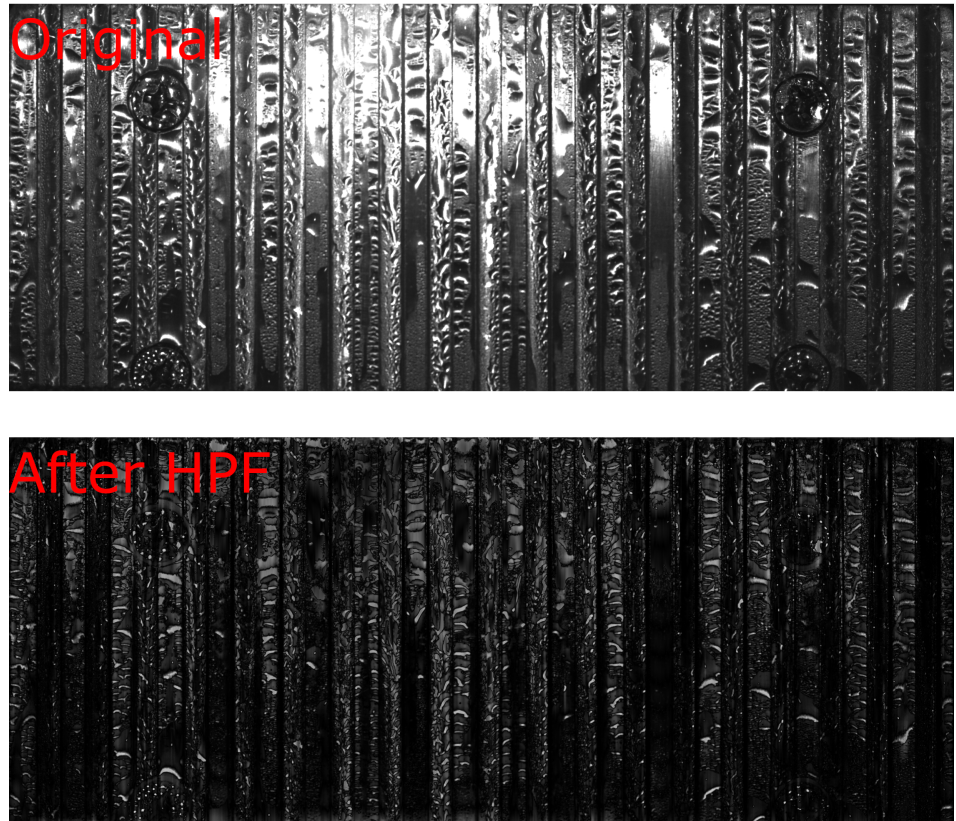
Figure 6. Image of the condenser before and after applying the high-pass filter.
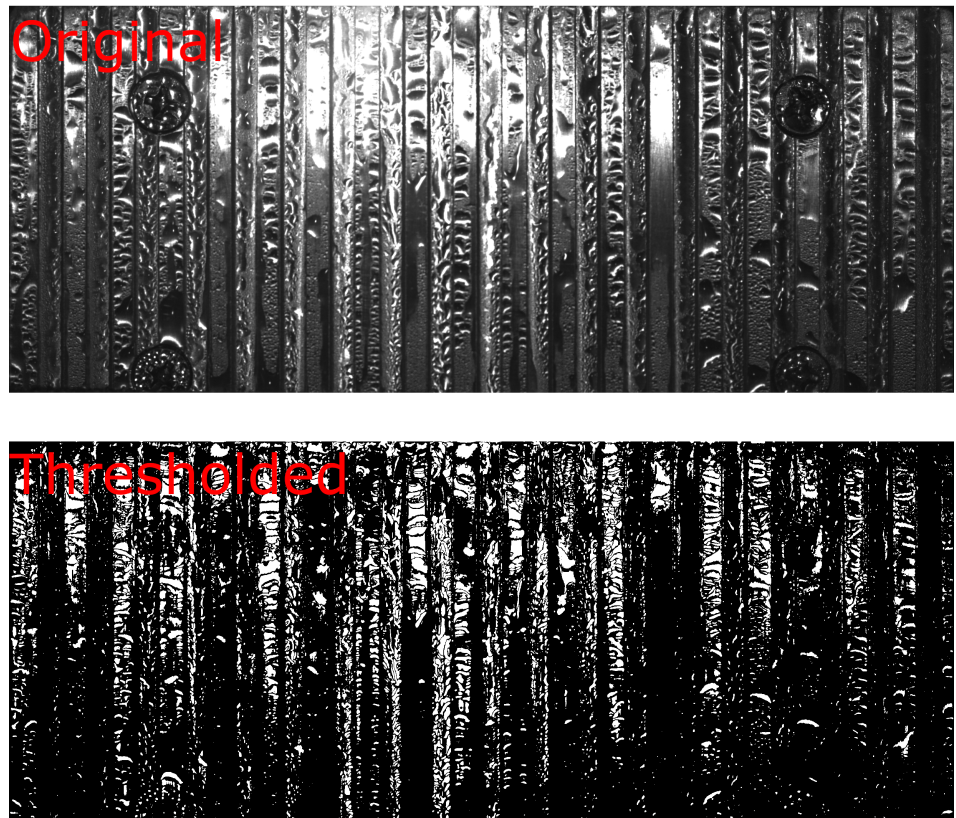

Figure 7. Image of the Condenser before and after Applying the High-Pass Filter and Thresholder by K-means.

3.2. Tuning For Individual Surfaces

There are no features in the y-direction with a similar spatial frequency to the droplets. In the x-direction (horizontal), however, the grooves have a spatial frequency not far from the droplets. The terms 'y-direction' and 'x-direction' refer to the orientation of the coordinates on the condenser plate. The 'x-direction' is aligned with the horizontal axis of the plate, while the 'y-direction' is aligned with the vertical axis. These directions are used to describe the spatial distribution and movement of the condensation patterns during the experiment. By analyzing the behavior of droplets along these axes, we can better understand the influence of gravity and other factors on the condensation process. Therefore, in the Fourier domain, a high-pass filter is constructed such that it only considers the spatial frequencies in the y-direction. Almost all the larger drops are not detected as one drop but as two separate segments with different colours very close to each other. This is a consequence of directional lighting. Consequently, drops appear as smaller drops and the volume is underestimated. To mitigate this effect, a k-means algorithm is used. Larger drops (empirically found to be defined as over 0.7 mm^2 in the area) are counted, with n-big drops being the total number and then grouped into n-big drops/2 clusters. Such clusters subsequently enter volume calculations as whole droplets. This is illustrated in Figure 8. An example of the overall result of the process is shown in Figure 9.

Figure 8. Sequence of Clustering the Drop Parts Starting From the Original Grooves Surface Image.

Figure 9. Example of the volume quantification on grooves.

Similarly, to the grooves, there is a feature with a similar x-direction spatial frequency to the droplets, but one must filter out the paths of the fallen droplets. The solution is to apply a high-pass filter devised in a way that only uses the y-direction. Another problem encountered was the bolts getting often detected with no droplets on them. Masking them manually solved this. Sometimes unrealistically large areas around the edges were also detected, and therefore, all drops with a size above an experimentally found threshold (found to be 115 mm^2) were filtered out. A typical process result on a hydrophobic surface is shown in Figure 10. In the case of a hydrophilic surface, all the features are very similar in the x and y-directions. Therefore, a high-pass filter is used to take both directions into

account. However, bolts have to be masked as they are getting detected. Areas above an empirically established threshold (70 mm^2) were filtered out. It was also found that better results were achieved if a morphological operation of dilation was applied after the thresholding. For the dilation, a 3 × 3 kernel was used. A '3 × 3 kernel' is a small matrix used in image processing to apply effects like blurring, sharpening, or edge detection. Each kernel value multiplies a corresponding pixel value in the image, and the results are summed to produce a new pixel value. The typical results are shown in Figure 11.
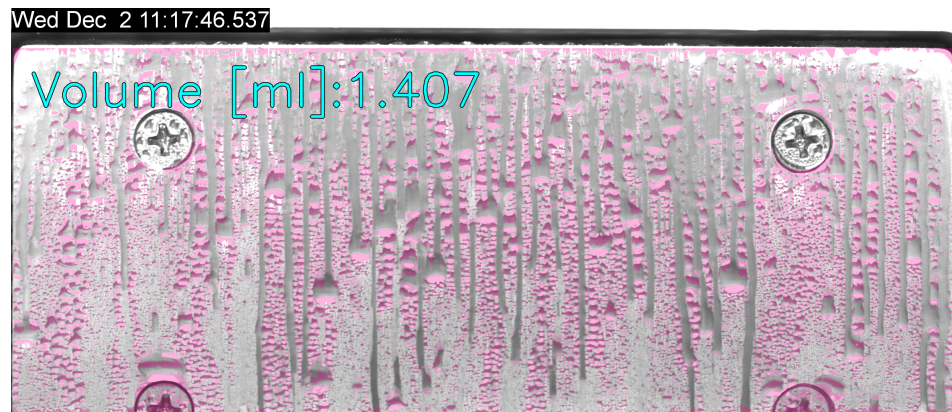

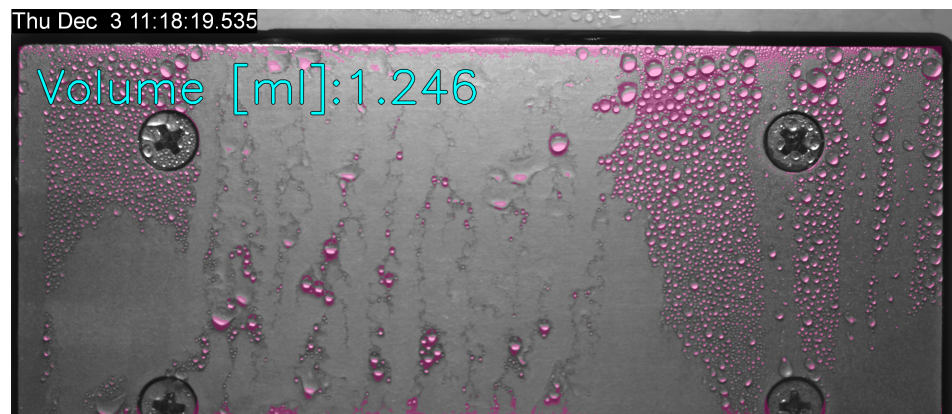**Figure 10.** Example of the volume quantification on a hydrophobic surface.

Figure 11. Example of the volume quantification on a hydrophilic surface.

4. Results

Figure 12a shows the measured temperature over the condensing surfaces during the first set of parabolas, while Figure 12b shows the temperature trend over the condensing surfaces during the second set of parabolas. As can be seen, the first set is indeed kept at about 10 °C, and the second at 15 °C. However, it can also be seen that fluctuations in the temperature of up to 2 °C are possible. As an example, the gravity levels corresponding to the first day (with the grooved substrate) are drawn in Figure 12 as well. During the hypergravity phase, the higher gravity pushes the condensed droplets to fall off the condenser, effectively cleaning it. This allows the condenser to be free again to absorb heat and condense more water vapor, leading to a decline in temperature and an oscillation as the system adjusts to the changing thermal load. The stationary conditions re-established at the end of the parabola caused temperatures to vary upwards, explaining the reason for the recorded temperature fluctuations. Figure 13 shows the measured condensed H_2O during the reduced-gravity intervals for the three substrates for all the parabolas. For each temperature (10 and 15 °C), each gravity level (Martian, lunar, microgravity), and each substrate (grooved, hydrophobic, and hydrophilic), the total amount of condensed H_2O is reported in Table 3.

First, we look at the overall results. Figure 13 shows that, for the grooved and hydrophobic substrates, a maximum amount of condensed H_2O occurs at microgravity, whereas this amount decreases as gravity increases. The overall tendency appears to be that the lower the gravity, the more H_2O is condensed. A numerical study shows that gravity plays a role in the vapor-liquid distribution [36].
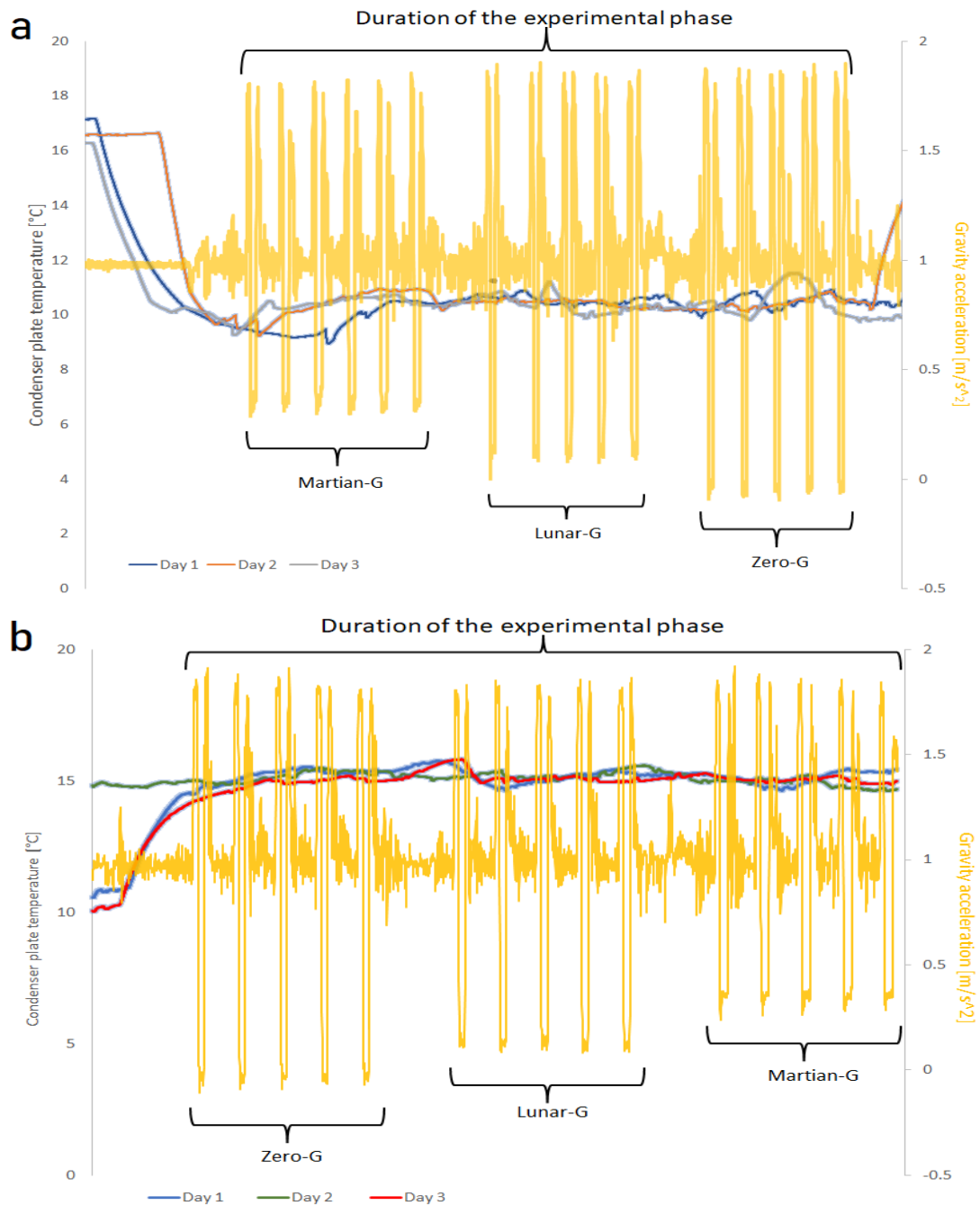

Figure 12. (**a**) The difference in temperature maintained during the experiment between the condenser plate and heat extraction system of the three days at a set temperature of 10 °C. (**b**) The difference in temperature maintained during the experiment between the condenser plate and heat extraction system of the three days at a set temperature of 15 °C.
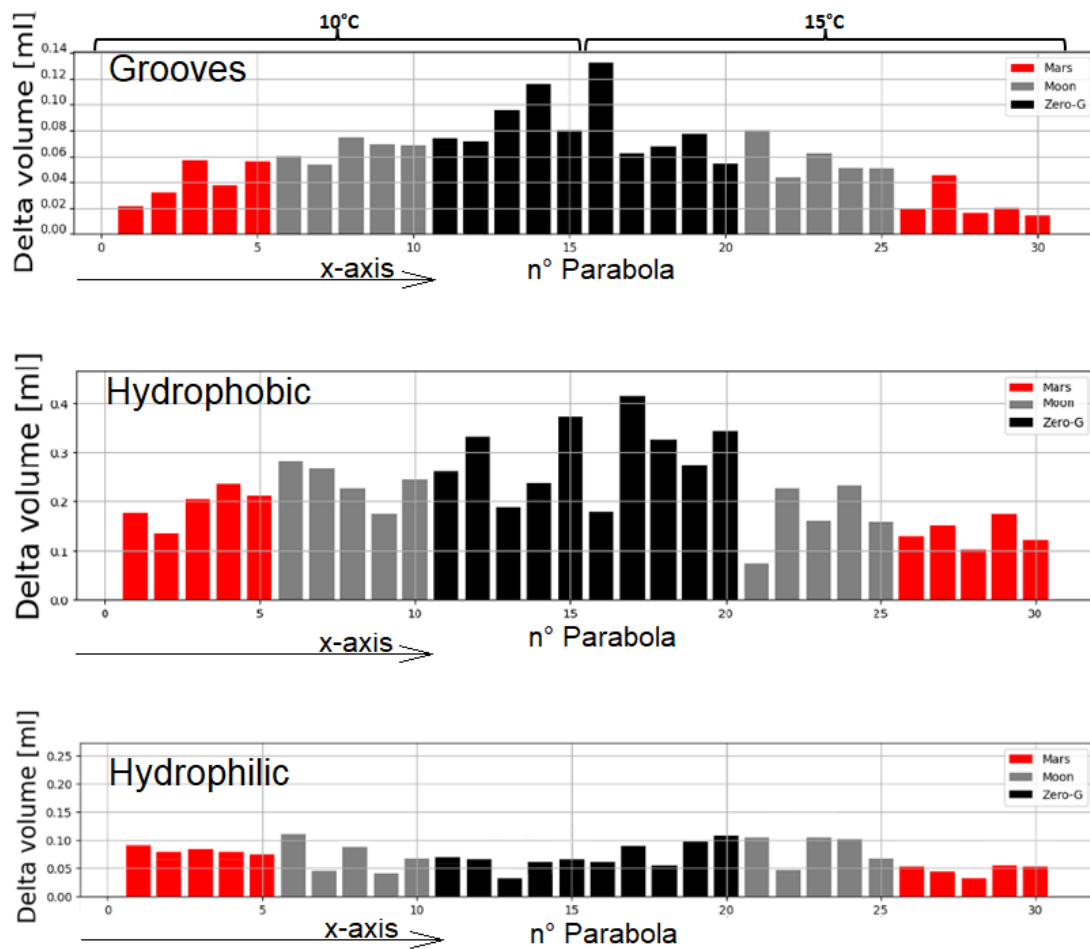
Figure 13. Water condensed in ml for each parabola experienced for each substrate.

Table 3. Volume of water condensed on the substrate after a series of 5 parabolas. Results are in ml of water condensed. The first table refers to condensation with the temperature of the substrate at 10 °C, and the second table refers to the temperature of the substrate at 15 °C. Standard deviations are included to indicate measurement variability.

Volume of Water in mL (Including Standard Deviations)			
10 °C	**Grooves**	**Hydrophobic**	**Hydrophilic**
Martian	0.18 ± 0.01	0.97 ± 0.05	0.45 ± 0.02
Lunar	0.33 ± 0.02	1.15 ± 0.06	0.37 ± 0.02
Zero-g	0.39 ± 0.02	1.36 ± 0.07	0.32 ± 0.01
Ground exp.	0.13 ± 0.01	0.31 ± 0.02	0.14 ± 0.01
15 °C	**Grooves**	**Hydrophobic**	**Hydrophilic**
Martian	0.13 ± 0.01	0.66 ± 0.03	0.23 ± 0.01
Lunar	0.29 ± 0.01	0.83 ± 0.04	0.38 ± 0.02
Zero-g	0.38 ± 0.02	1.26 ± 0.06	0.43 ± 0.02
Ground exp.	0.10 ± 0.01	0.27 ± 0.02	0.12 ± 0.01

Finally, the effect of temperature is quite clear. Table 3 shows that a higher substrate temperature results in less condensed water. This is understood by reminding us that at a higher temperature, the saturation pressure is also higher, resulting in a thermodynamic equilibrium favoring more vapor in the gas phase and, therefore, less condensate.

The results from the ground experiments indicate a consistent performance in water extraction across different surface types. The error analysis, presented in Table 4, shows

the mean and standard deviation of water extracted for each surface type. The standard deviations are relatively low, indicating minimal variability in the data. This suggests that the results are reliable and the experimental setup is robust.

Table 4. Water extracted by surface type during a sequence of 10 ground experiments.

Surface Type	Mean Water Extracted (mL)	Standard Deviation (mL)
Groove	11.125	1.190
Hydrophobic	28.25	0.925
Hydrophilic	11.875	0.479

5. Discussions

A numerical study shows that gravity plays a role in the vapor-liquid distribution [36].

The successful execution of in-situ resource utilization (ISRU) technologies hinges on understanding fluid dynamics under varied gravitational conditions. Our study, conducted during the 74th ESA parabolic flight campaign, explored the efficiency of water recovery from regolith analogs in simulated lunar and Martian gravities. These types of findings are important for the development of sustainable extraterrestrial habitats. Our experiments highlighted the influence of gravity on condensation efficiency, with lower gravity environments favoring higher condensation rates. This enhanced condensation in microgravity can be attributed to decreased mechanical resistance against the phase transition of water molecules. Among the substrates tested—hydrophobic, hydrophilic, and grooved—the hydrophobic surface demonstrated the highest water recovery efficiency. This substrate's tendency to promote drop-wise condensation "(condensation that forms discrete droplets rather than a continuous film, which resulted in higher heat transfer from the condensed H_2O droplets to the condenser surface and, thus, water recovery, points to the potential of material engineering in optimizing ISRU technologies. Furthermore, the incorporation of porous media effectively managed fluid dispersal across varying gravity phases, maintaining the integrity and consistency of water recovery. This strategic integration highlights the necessity for advanced system engineering in ISRU technologies to address the complexities of fluid management in space. Future research should aim to refine these systems through extended material studies and advanced prototypes, potentially in actual space missions. Testing these technologies under real space conditions will validate their long-term stability and efficiency, crucial for developing reliable life support systems on the Moon and Mars. This research contributes significantly to the field of ISRU by advancing our understanding of water recovery in space. It offers a foundational step towards achieving long-term human presence on extraterrestrial bodies.

Our error analysis for ground experiments, shown in Table 4, validates our findings. The standard deviation values indicate consistent trends across substrate types, reinforcing the reliability of our data. The observed differences in condensation efficiency, particularly the superior performance of the hydrophobic substrate, are statistically significant.

The groove substrate exhibited higher variability in water extraction, suggesting the need for further refinement. Conversely, the hydrophobic surface showed the lowest standard deviation, indicating robustness and efficiency.

The pressure conditions during the parabolic flight, while not lunar-like, simulated the closed-system operations necessary for efficient water extraction. Future studies should replicate these experiments at lunar-like pressures for enhanced relevance.

Our experiments revealed that substrate properties play a more crucial role than gravity levels in determining water recovery efficiency. This underscores the importance of selecting and engineering appropriate materials for ISRU applications. The consistency observed in ground experiments validates our findings despite limited repetitions during parabolic flights.

6. Conclusions

The proposed experiment focuses on extracting and condensing water as a preliminary step towards improving the efficiency of water extraction from lunar regolith. To determine the most efficient surface, three types of substrates were selected and evaluated (groove, hydrophobic, and hydrophilic). A thermal extraction was implemented, with each component undergoing initial testing under terrestrial conditions for parabolic flight suitability. This process not only validated the feasibility of the water collection system but also confirmed the potential use of these surfaces for future water extraction. Future implementations will require the addition of a water retraction pump and a reclaimed water storage container. During the parabolic flight, the condensation surfaces (grooves, hydrophobic, hydrophilic) were tested while maintaining an identical global configuration across three days. Observable differences in condensing capacity led to the conclusion that a hydrophobic substrate demonstrated a superior ability to convert vapor into liquid under the same experimental conditions.

Subsequent ground experiments conducted after the parabolic flight yielded lower water vapor condensation results compared to the flight experiments. However, the hydrophobic surface generally exhibited the best condensation performance. Additionally, the results indicated that condensation efficiency was dependent on the surface properties of the condenser as well as the gravity level experienced during the experiment. Three gravity levels were used for the experimental tests: Martian, lunar, and micro-gravity. The highest condensation was observed in micro-gravity conditions, followed by lunar gravity and then Martian gravity. This straightforward approach using a thermal condenser holds promise as an in-situ resource utilization (ISRU) method for water extraction. However, various factors, such as the heating method, power level, and ice fraction, influence the extraction process. The experimental setup presented in this study could be implemented for extracting water from lunar regolith, and the insights gained from the results contribute to our understanding of thermal water extraction as an ISRU approach. In conclusion, this experiment demonstrated the efficiency of a thermal condenser in extracting water from lunar regolith under different gravity levels and surface properties. The findings provide valuable insights into the parameters impacting condensation efficiency and rate, which can guide future research and development of thermal condensers for water extraction. The values presented in Table 3 are considered accurate as they fall within the tolerance range of our measurement system. This experiment provides a first overview of our outcomes using this new system, which will be further implemented and refined based on these initial results. Further investigation will delve into the analysis of sublimation under various gravities using different condensation substrates.

students, Nadine Karaouni and Ondřej Dvořák, for their persistent assistance and unwavering commitment throughout this project.

Abbreviations

The following abbreviations are used in this manuscript:

ISRU	In-Situ Resource Utilization
LCROSS	Lunar Crater Observation and Sensing Satellite
LRO	Lunar Reconnaissance Orbiter
SOFIA	Stratospheric Observatory for Infrared Astronomy
MTCS	Methyltrichlorosilane
PVA	Polyvinyl Alcohol
MMT	Montmorillonite
PMA	Polyvinyl Alcohol-Montmorillonite Aerogel
HPMA	Highly Porous Montmorillonite Aerogel
CVD	Chemical Vapor Deposition
ESA	European Space Agency
NASA	National Aeronautics and Space Administration
ATM	Aero-Thermo-Mechanics
ULB	Université Libre de Bruxelles
CREST	Centre for Research and Engineering in Space Technologies
DSA30	Drop Shape Analyzer 30

References

1. Mitrofanov, I.G.; Sanin, A.B.; Boynton, W.V.; Chin, G.; Garvin, J.B.; Golovin, D.; Evans, L.G.; Harshman, K.; Kozyrev, A.S.; Litvak, M.L.; et al. Hydrogen mapping of the lunar south pole using the LRO neutron detector experiment LEND. *Science* **2010**, *330*, 483–486. https://doi.org/10.1126/science.1185696.
2. Shkuratov, Y.G.; Bondarenko, N.V. Regolith layer thickness mapping of the Moon by radar and optical data. *Icarus* **2001**, *149*, 329–338. https://doi.org/10.1006/icar.2000.6537.
3. Smith, P.H.; Tamppari, L.K.; Arvidson, R.E.; Bass, D.; Blaney, D.; Boynton, W.V.; Carswell, A.; Catling, D.C.; Clark, B.C.; Duck, T.; et al. H$_2$O at the Phoenix landing site. *Science* **2009**, *325*, 58–61. https://doi.org/10.1126/science.1172339.
4. Crawford, I.A. Lunar resources: A review. *Prog. Phys. Geogr.* **2015**, *39*, 137–167. https://doi.org/10.1177/0309133314567585.
5. Metzger, P.T. Affordable, rapid bootstrapping of the space industry and solar system civilization. *New Space* **2016**, *4*, 185–194. https://doi.org/10.1089/space.2016.0018.
6. Cole, J.D.; Lim, S.; Sargeant, H.M.; Sheridan, S.; Anand, M.; Morse, A. Water extraction from icy lunar simulants using low power microwave heating. *Acta Astronaut.* **2023**, *209*, 95–103. https://doi.org/10.1016/j.actaastro.
7. Sargeant, H.M.; Barber, S.J.; Anand, M.; Abernethy, F.A.J.; Sheridan, S.; Wright, I.P.; Morse, A.D. Hydrogen reduction of lunar samples in a static system for a water production demonstration on the Moon. *Planet. Space Sci.* **2021**, *205*, 105287. https://doi.org/10.1016/j.pss.2021.105287.
8. Clark, R.N. Detection of Adsorbed Water and Hydroxyl on the Moon. *Science* **2009**, *326*, 562–564.
9. Paige, D.A.; Siegler, M.A.; Zhang, J.A.; Hayne, P.O.; Foote, E.J.; Bennett, K.A.; Vasavada, A.R.; Greenhagen, B.T.; Schofield, J.T.; et al. Diviner lunar radiometer observations of cold traps in the Moon's south polar region. *Science* **2010**, *330*, 479–482.
10. Kereszturi, A. Polar Ice on the Moon. In *Encyclopedia of Lunar Science*; Cudnik, B., Ed.; Springer: Cham, Switzerland, 2023. https://doi.org/10.1007/978-3-319-14541-9_216.
11. Levrard, B.; Forget, F.; Montmessin, F.; Laskar, J. Recent ice-rich deposits formed at high latitudes on Mars by sublimation of unstable equatorial ice during low obliquity. *Nature* **2004**, *431*, 1072–1075. https://doi.org/10.1038/nature03055.
12. Arvidson, R.E. Aqueous history of Mars as inferred from landed mission measurements of rocks, soils, and water ice. *J. Geophys. Res. Planets* **2016**, *121*, 1602–1626.
13. Changela, H.G.; Chatzitheodoridis, E.; Antunes, A.; Beaty, D.; Bouw, K.; Bridges, J.C.; Capova, K.A.; Cockell, C.S.; Conley, C.A.; Dadachova, E.; et al. Mars: New insights and unresolved questions—Corrigendum. *Int. J. Astrobiol.* **2022**, *21*, 46. https://doi.org/10.1017/S1473550421000380.
14. Li, S.; Milliken, R.E. Direct Evidence of Surface Exposed Water Ice in the Lunar Polar Regions. *PNAS* **2017**, *114*, 201701147.
15. Honniball, C.I.; Lucey, P.G.; Li, S.; Shenoy, S.S.; Orlando, T.M.; Hibbitts, C.A.; Hurley, D.M.; Young, E.F. Molecular water detected on the sunlit Moon by SOFIA. *Nat. Astron.* **2021**, *5*, 121–127. https://doi.org/10.1038/s41550-020-01222-x.
16. Liu, Y.; Guan, Y.; Zhang, Y.; Rossman, G.R.; Eiler, J.M. Direct Measurement of Hydroxyl in the Lunar Regolith and the Origin of Lunar Surface Water. *Nat. Geosci.* **2012**, *5*, 779–782.

17. Schrunk, D.; Sharpe, B.; Cooper, B.L.; Thangavelu, M. *The Moon: Resources, Future Development and Settlement*; Springer Science & Business Media: Berlin/Heidelberg, Germany, 2007.

18. Boazman, S.; Kereszturi, A.; Heather, D.; Sefton-Nash, E.; Orgel, C.; Tomka, R.; Houdou, B.; Lefort, X. Analysis of the Lunar South Polar Region for PROSPECT. In Proceedings of the Europlanet Science Congress 2022, Palacio de Congresos de Granada, Spain, 18–23 September 2022.

19. Showstack, R. Lunar prospector finds signature for water ice on Moon, NASA announces. *Eos, Transactions American Geophysical Union* **1998**, *79*, 138–144.

20. Keller, J.W.; Petro, N.E.; Vondrak, R.R. The Lunar Reconnaissance Orbiter Mission – Six years of science and exploration at the Moon. *Icarus* **2016**, *273*, 2–24. https://doi.org/10.1016/j.icarus.2015.11.024.

21. Gallbrecht, M.M.; Cervone, A.; Vincent-Bonnieu, S. The Moon as an effective propellant source: A comprehensive exergy analysis from extraction to depot. *Acta Astronaut.* **2024**, *52*, 307–313.

22. Pál, B.; Kereszturi, Á.; Möhlmann, D.; Berczi, S.; Gucsik, A.; Sik, A. Global seasonal variations of the near-surface relative humidity levels on present-day Mars. *Icarus* **2019**, *333*, 481–495. https://doi.org/10.1016/j.icarus.

23. Sanders, G.B.; Larson, W.E. Progress Made in Lunar In-Situ Resource Utilization under NASA's Exploration Technology and Development Program. *J. Aerosp. Eng.* **2018**, *31*, 04018020. https://doi.org/10.1061/(ASCE)AS.1943-5525.0000208.

24. Liu, Y.; Wang, C.; Pang, Y.; Wang, Q.; Zhao, Z.; Lin, T.; Wang, Z.; Shen, T.; Liu, S.; Song, J.; et al. Water Extraction from Icy Lunar Regolith by Drilling-Based Thermal Method in a Pilot-Scale Unit. *Acta Astronaut.* **2023**, *202*, 386–399.

25. Spudis, P.D.; Bussey, D.B.J.; Baloga, S.; Cahill, J.T.S.; Crusan, J. Extracting water from lunar polar ice: Results of the Lunar Crater Observation and Sensing Satellite mission. *J. Geophys. Res. Planets* **2013**, *118*, 2016–2029. https://doi.org/10.1002/jgre.20156.

26. Heiken, G.; Vaniman, D.; French, B.M. *Lunar Sourcebook: A User's Guide to the Moon*; Cup Archive: Cambridge, UK, 1991.

27. Purrington, C.; Sowers, G.; Dreyer, C. Thermal Mining of Volatiles in Lunar Regolith Simulant. *Planet. Space Sci.* **2022**, *222*, 105550. https://doi.org/10.1016/j.pss.2022.105550.

28. Ethridge, E.C. Microwave Heating of Lunar Regolith for Water Extraction. *J. Aerosp. Eng.* **2009**, *22*, 53–61.

29. Zhang, X. Hydrothermal Processes in Martian Regolith: Experiments and Applications. *J. Geophys. Res. Planets* **2008**, *113*, E06003.

30. Sanders, G.; Larson, W.; Sacksteder, K.; Mclemore, C. NASA in-situ resource utilization (ISRU) project: Development and implementation. In Proceedings of the AIAA SPACE 2008 Conference & Exposition, San Diego, CA, USA, 9–11 September 2008.

31. Sowers, G.F.; Dreyer, C.B.; Sanders, G.B. A Cislunar Transportation System Fueled by Lunar Resources. *Space Policy* **2016**, *37*, 103–109. https://doi.org/10.1016/j.spacepol.2016.07.001.

32. Barakhovskaia, E.; Glushchuk, A.; Queeckers, P.; Iorio, C.S. Stabilisation of condensate flow from curvilinear surfaces by means of porous media for space applications. *Exp. Therm. Fluid Sci.* **2021**, *121*, 110283. https://doi.org/10.1016/j.expthermflusci.2020.110283.

33. Berto, A.; Azzolin, M.; Lavieille, P.; Glushchuk, A.; Queeckers, P.; Bortolin, S.; Iorio, C.S.; Miscevic, M.; Del Col, D. Experimental investigation of liquid film thickness and heat transfer during condensation in microgravity. *Int. J. Heat Mass Transf.* **2022**, *199*, 123467. https://doi.org/10.1016/j.ijheatmasstransfer.2022.123467.

34. Shakeri Bonab, M.; Minetti, C.; Iorio, C.S.; Zhao, D.; Liu, Q.-S.; Ou, J.; Kempers, R.; Amirfazli, A. Experimental investigation of dropwise condensation shedding by shearing airflow in microgravity using different surface coatings. *Langmuir* **2022**, *39*, 64–74. https://doi.org/10.1021/acs.langmuir.2c01898.

35. Duta, L.; Popescu, A.; Zgura, I.; Preda, N.; Mihailescu, I. Wettability of nanostructured surfaces. *Wetting Wettability* **2015**, *8*, 207–252.

36. Gu, X.; Wen, J.; Tian, J.; Li, C.; Liu, H.; Wang, S. Role of gravity in condensation flow of R1234ze(E) inside horizontal mini/macro-channels. *Exp. Comput. Multiph. Flow* **2019**, *1*, 219–229.